P91

DEVELOPMENT AND EVALUATION OF THE SECOND HURRICANE NATURE RUN USING THE JOINT OSSE NATURE RUN AND THE WRF MODEL

David S. Nolan* and Craig A. Mattocks+
Rosenstiel School of Marine and Atmospheric Science
University of Miami, Miami, Florida

1. **INTRODUCTION**

A "nature run" is an integral component of an observing system simulation experiment (OSSE), which is a framework for assessing the potential impact of additional observations, new observing systems, or new data assimilation schemes in improving numerical weather forecasts. In this approach, a high-quality simulation of a period of weather or a weather event of interest is used as a "truth" or "nature" data set. Initial conditions and synthetic observations are generated from the nature run and are provided to a forecast model. The impact of new observations or new schemes can be measured by the extent to which they cause the forecasts to more accurately reproduce the nature run event (Atlas 1997). Some advantages of the OSSE approach over case studies is that 1) the differences between the forecasts and the truth can be known exactly, 2) new observations, even from hypothetical instruments that do not yet exist, can be generated from the nature run, and 3) varying configurations and densities of existing or hypothetical measurements can be evaluated to find optimal observing strategies.

A hurricane nature run was previously generated and extensively validated by Nolan et al. (2013, hereafter N13). That simulation, hereafter referred to as HNR1, depicts the entire life cycle of an Atlantic hurricane from initiation as an African easterly wave, to tropical cyclogenesis, to rapid intensification, and finally to recurvature over the North Atlantic. This data set is currently in use for a variety of purposes, including OSSEs for hurricane forecasts using one of the NOAA operational hurricane forecast models (HWRF), as a source of realistic surface winds fields for evaluation of observing systems (Nolan et al. 2014), and for investigating physical processes (Kepert and Nolan 2014).

* Corresponding author address: Prof. David S. Nolan, RSMAS/MPO, 4600 Rickenbacker Causeway, Miami, FL 33149. email: dnolan@rsmas.miami.edu

+ Current affiliation: NOAA/National Hurricane Center, Miami, FL.

This paper describes the development and evaluation of a second hurricane nature run, hereafter referred to as HNR2. Like HNR1, the initial and boundary conditions for this regional simulation are provided by global fields from a global nature run previously generated by ECMWF using their weather forecast model in a free-running mode, forced by observed SSTs during a 13 month period from 2005 to 2006 (Reale et al. 2007; Masutani et al. 2009). This global simulation is known as the Joint OSSE Nature Run (JONR). Following N13, a tropical cyclone depicted during the JONR hurricane season was selected for regional downscaling.

2. **CASE SELECTION AND ANALOG STORMS**

The simulation period was chosen to range from 12Z August 20 to 12Z August 28 2005 of the JONR simulation. During this time, a tropical wave with an identifiable surface low pressure center approaches the northeast Caribbean and passes directly over Puerto Rico and Hispaniola. Despite significant land interactions, it then intensifies between Haiti and Cuba, traverses the length of Cuba as a weak cyclone, and then emerges in the Florida Straits near Havana. The cyclone then rapidly intensifies as it travels northward before making landfall near Tampa, Florida. The path of the JONR cyclone is shown in Fig. 1. The strong land interactions and ultimately the landfall in Florida make this case of interest, particularly in contrast to HNR1.

The path of this storm is similar to innumerable waves, disturbances, and weak tropical storms that have passed through this region over the last 100 years. While it is unusual for a storm to form and/or maintain tropical storm intensity while interacting with the Greater Antilles, it has happened on a number of occasions. The paths of two analog storms, Frederic (1979) and Elena (1985) are also shown in Fig. 1. Both of these systems maintained intensity despite their interactions with the large islands of the Caribbean. Although it had previously achieved hurricane status, Frederic weak-

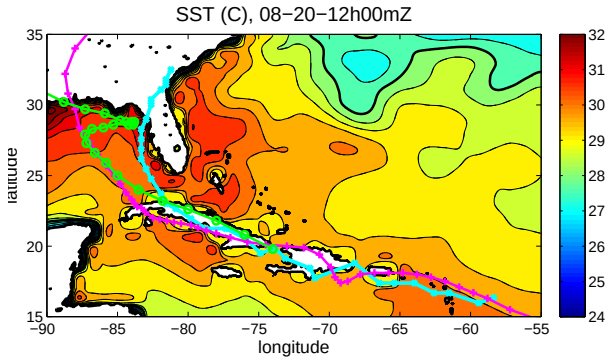

Fig. 1: Land distribution and initial sea surface temperature (SST) for HNR2. Also shown are the path of the simulated tropical cyclone in the JONR (cyan curve) and the tracks of Hurricane Frederic (1979) (magenta) and Hurricane Elena (1985) (green). The SST contour interval is 0.5C and the 28C contour is thickened.

ened to tropical storm strength before it passed over Hispaniola, weakened to a depression between Haiti and Cuba, maintained depression status as it moved along the south edge of Cuba, and then intensified to a tropical storm again while over the west end of the island. Elena was identified as a depression while in the Windward Passage, very near to where a closed surface circulation first forms in HNR2 (see below). Elena achieved tropical storm strength while still over the north edge of Cuba.

3. **MODELING STRATEGY**

For HNR2, WRF was updated from version 3.2.1 to version 3.4.1. Drawing from the success of HNR1, many settings and parameters in the WRF model remained the same for HNR2. These include 60 vertical levels with the same distribution, the Kain-Fritsch cumulus scheme on the outer grid, the WSM6 double moment microphysics on all grids, the RRTM-G radiation scheme called every 5 min (previously every 6 min) on all grids, and the YSU PBL scheme, with the formula for drag coefficient as a function of wind speed reverted back to the WRF 3.1.1 version. Newtonian relaxation of the model fields on the WRF outer domain toward the global fields of the JONR (also known as “grid nudging”) with a 24 hour time scale was also used.

A significant change is that the outer domain resolution was changed from 27 km to 9 km, and there were only two vortex-tracking moving nests using 3 km and 1 km grid spacing. This allowed the

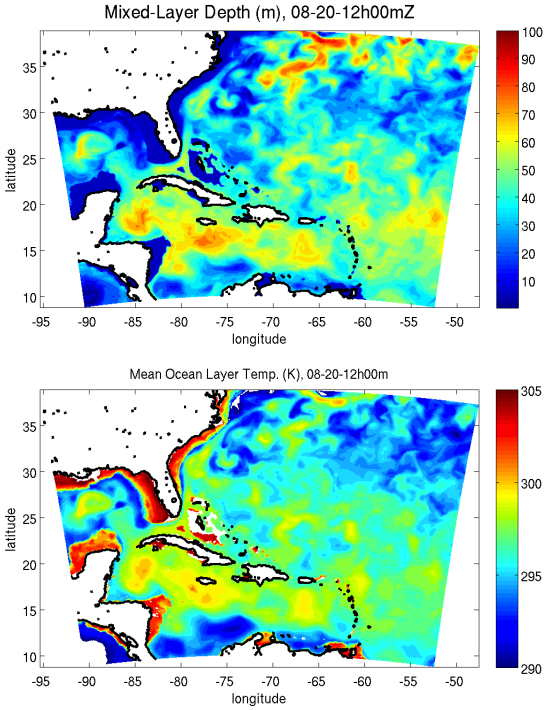

Fig. 2: Input data for the simple mixed-layer ocean temperature model: initial mixed-layer depth (top) taken from a HYCOM analysis on the same date in 2005; the mean upper-ocean temperature (bottom), which sets a lower limit on the cooling that can be achieved by wind-stress induced mixing.

underlying coastlines, topography, and land-use fields to be better represented at 9 km resolution. The domain sizes are 480x360, 360x360, and 480x480 points. Note the size of the 3 km domain matches the size of the 9 km domain in HNR1, thereby keeping the effects of “nudging” to at least 540 km from the storm center, again as in HNR1.

Another change is the use of more realistic fields of ocean mixed layer depths and temperatures. Rather than constant mixed layer depth and stratification as used in HNR1, realistic fields were derived from a HYCOM ocean model analysis of ocean temperature profiles taken from 12Z August 20 2005. This was done so that ocean mixed layer cooling due to wind stresses from the storm could be more realistically simulated by the one-dimensional mixed-layer cooling scheme of Pollard et al. (1973), particularly as the cyclone passed over the Florida straits and into the eastern Gulf of Mexico. Fig. 2 shows the fields of mixed layer depth and mean mixed layer temperature used to initialize the one-dimensional mixed-layer model at each grid

point. The mean mixed layer temperature defines a lower limit below which the surface temperature cannot fall due to mixed-layer cooling caused by wind stress. Note that the entire model domain (9 km grid) is shown in these plots.

The actual SST values came from the surface (skin) temperatures of the JONR at 12Z August 20. These fields had colder surface temperatures on the poorly resolved islands that projected onto the ocean surface when interpolated to the 9 km resolution land mask. Areas around the Caribbean islands and Florida that had SSTs less than 29C were raised to 29C, and then the fields were locally averaged repeatedly with surrounding data for smooth transitions into the surrounding ocean temperatures. Nonetheless, some circular patches of slightly cooler SSTs are evident, such as around Puerto Rico and the western tip of Cuba (see Fig. 1).

An additional change was the use of the Noah land surface model (see, e.g., Chen and Dudhia 2001) in place of the simple thermal diffusion model used in HNR1. Initial fields required by NOAH LSM, such as soil temperature and soil moisture for the 4 resolved layers, were extracted from the JONR output files and used for initialization.

4. **CYCLONE EVOLUTION**

The track and intensity of the hurricane simulated in the second nature run, which hereafter is referred to as NRH2 (HNR2 is the simulation, NRH2 is the storm), are shown in Fig. 3. Much like the JONR cyclone from the same period, the NRH2 disturbance passes over Puerto Rico and Hispañola, intensifies between Haiti and Cuba, travels much of the length of Cuba, and then after a period of rapid intensification strikes the west coast of Florida. After landfall north of Tampa, NRH2 traverses Florida and eastern Georgia, moves over the ocean briefly, and then becomes stationary in South Carolina.

The intensity evolution shows four stages: pregenesis, a slowly intensifying tropical storm, rapid intensification to a category 2 hurricane, and then decay after landfall. Surprisingly, the minimum surface pressure falls to lower values for the JONR cyclone, but this is likely due to the much larger size of the wind field due to substantially larger

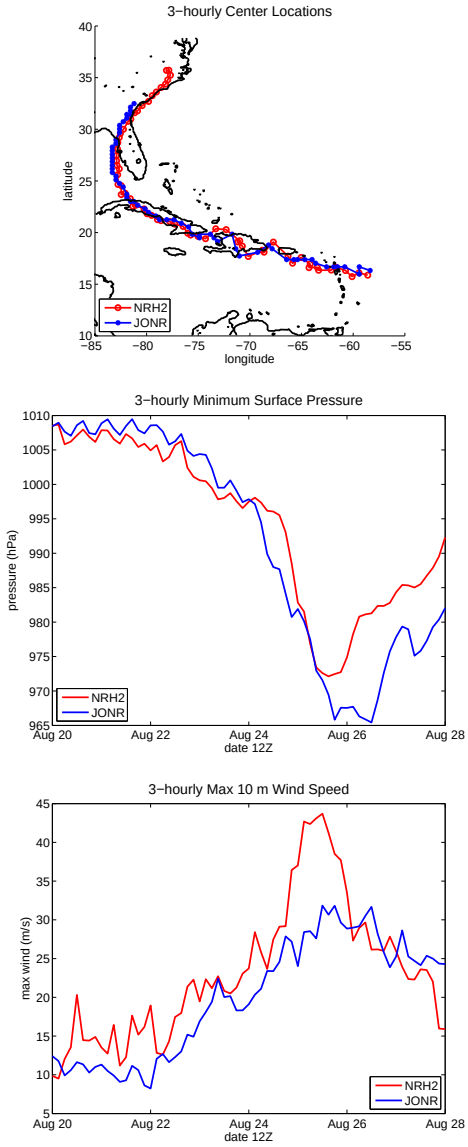

Fig. 3: Track (top), minimum surface pressure (middle) and peak surface (10 m) wind speed every 3 h for the JONR cyclone (blue) and NRH2 (red). In these figures, data for NRH2 are from instantaneous outputs from the 1 km grid every 3 hours.

effective grid spacing in the ECMWF model.

The wind speed plot shows the peak surface (10 m) wind speed from the 1 km grid every 3 hours, suggesting a peak intensity of 43 ms^{-1}. However, as discussed in section 4.3 of N13, this can be deceptive, since there can be enormous variability in the instantaneous peak surface winds from hour to hour, or even minute to minute. To illustrate this point, Fig. 4 shows four values: the peak surface wind from the 1 km grid, every 5 min-

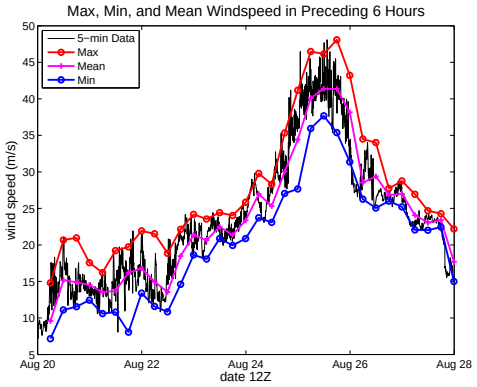

Fig. 4: Various measures of representative intensity for NRH2: 5-minute output from the 1 km grid, adjusted to 1 min means, and their maximum, minimum, and mean values over each preceding 6 hour period.

utes, adjusted by a gust-factor formula to equivalent one-minute mean values (see section 4.3 of N13); and the maximum, minimum, and mean value of this wind speed in the preceding 6 hours. The mean value indicates a more representative peak intensity, consistent with the definition of the "best track" intensity (Landsea and Franklin 2013), of just over 40 ms^{-1}.

The fact that NRH2 maintains tropical storm intensity while interacting with Cuba can be understood by considering its larger environment. Fig. 5 shows the mean 850 to 200 hPa vertical wind shear in a 900km x 900km box centered on the mid-level circulation, along with the SST in the same region (with land surface values excluded). After the first 24 h, shear becomes less than 7.5 ms^{-1} and occasionally decreases to less than 5

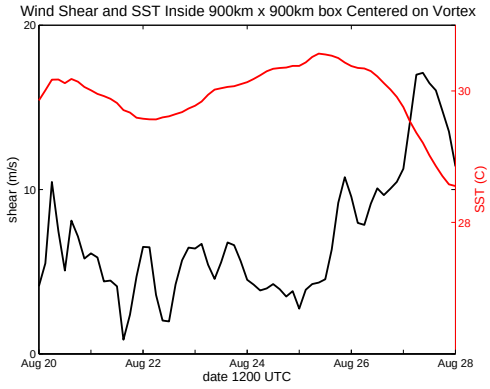

Fig. 5: 850 to 200 hPa wind shear (black) and SST (red) in a 900 km x 900 km box following the storm. Land surface temperatures are excluded.

ms^{-1} while the storm is over Cuba. The surrounding ocean temperatures remain above 29.4C.

While a broad surface low can be tracked dur-

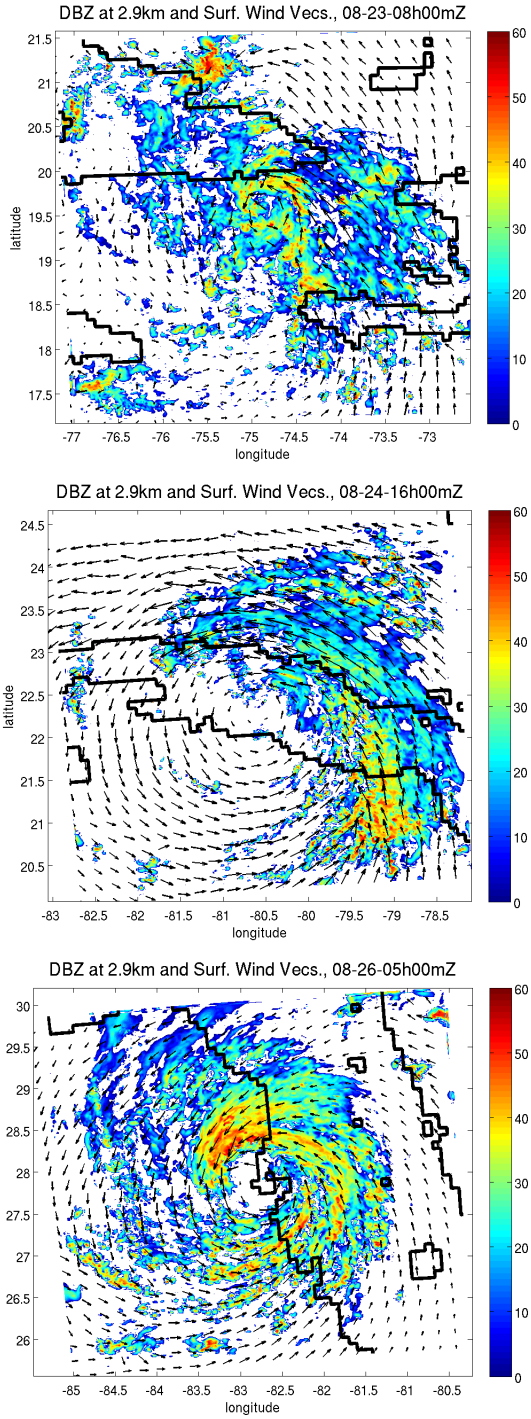

Fig. 6: Simulated reflectivity at z = 2.9 km and surface wind vectors at selected times during the evolution of NRH2. In the first plot, wind vectors are scaled so that one reaching its neighbor indicates 20 ms^{-1}. In the subsequent plots, this indicates 40 ms^{-1}.

ing the first few days of the simulation, a coherent surface circulation does not appear until the mid-level circulation moves over the ocean just west of Haiti. Fig. 6 shows simulated reflectivity and surface wind vectors at the first hourly time when a closed circulation can be identified at the surface. Other times of interest are also shown in Fig. 6, such as when the storm is over central Cuba and when the hurricane eye is directly over St. Petersburg, Florida.

5. PRESSURE-WIND RELATIONSHIP

Historical data bases of minimum surface pressure and estimated maximum surface wind speed show a distinct relationship between these two measures of hurricane intensity, although there is considerable scatter about this relationship (Atkinson and Holliday 1977; Knaff and Zehr 2007). A number of studies have used simulated pressure-wind relationships to evaluate the realism of simulated storm structure (e.g., Moon et al. 2007; Bao et al. 2012; Tallapragada et al. 2014). Here we again follow N13: peak winds from the 1 km grid, adjusted to 1-min mean winds, are plotted against their minimum pressure values every 30 min and compared to previously developed empirical pressure-wind relationships of Atkinson and Holliday (1977), Dvorak (1984), and Knaff and Zehr (2007). In this case, the Knaff and Zehr parameter for environmental pressure, mean surface pressure between 800 and 1000 km radius from the storm, had to be disregarded since that area extended beyond the computational domain for much of the simulation. Instead, an arbitrary, fixed value of 1013 hPa was used.

Fig. 7 shows the simulated pressure-wind relationship for NRH2. Only data from the period from 12Z August 23 to 12Z August 26 is shown, approximately from when the cyclone reaches tropical storm strength to the time of final landfall north of Tampa Bay (see Fig. 3). This includes the period when the storm was traveling over Cuba. While normally land-interaction points are excluded from pressure-wind analyses, the data points from when NRH2 is interacting with Cuba (blue points) are in fact closer to the Knaff and Zehr (2007) pressure-wind formula than when the cyclone re-emerges over the ocean. While the storm intensifies, the simulated wind values are higher than the surface pressure would be expected to indicate. This was

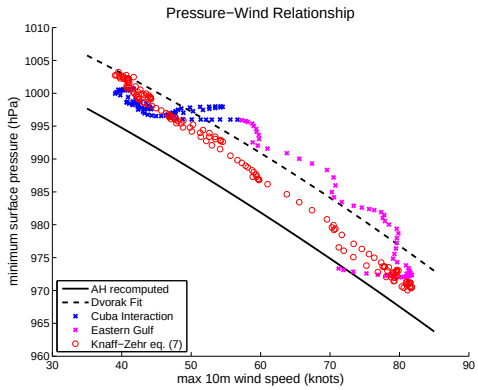

Fig. 7: Wind-pressure relationship for peak surface winds adjusted to 1-min means versus minmum surface pressure, and also cmpared to the Dvorak, Atkinson and Holliday, and Knaff-Zehr pressure-wind relationships. See text for details.

also true during the intensification phase of NRH1 (see Fig. 14 of N13), suggesting that this could either be a feature of intensifying storms or an artifact shared by both simulations.

6. BOUNDARY LAYER STRUCTURE

N13 showed time-composited, azimuthal-mean structures of the boundary layer of NRH1 and compared them to boundary layer composites derived from hundreds of dropsonde profiles accumulated over many hurricanes as presented by Zhang et al. (2011). The comparisons were quite good, with the simulated boundary layer being a bit too deep and the surface tangential winds being too strong (in comparison to the observed fields).

For NRH2, such comparisons are complicated by the significant land interactions. Fig. 8 shows azimuthal mean fields of V_t, V_r, and θ_v composited from the 3 km grid over 3 hours ending at 18Z August 25, when the storm was near its peak intensity and still fairly far from the Florida coast. V_t and V_r are normalized by their peak values, while the radial coordinate is rescaled by the radius of maximum winds (RMW) at z = 2 km. θ_v is rescaled but not normalized. Comparisons of these figures to the results shown in Zhang et al. (2011) and N13 indicate that the boundary layer of NRH2 has very similar biases as NRH1: the depth of the inflow layer and the height the peak V_t are too large and the V_t values near the surface are too strong. Unlike in HNR1 (and the observational data), V_r is maximized at considerably greater distance from the storm center than V_t. This may be due to the

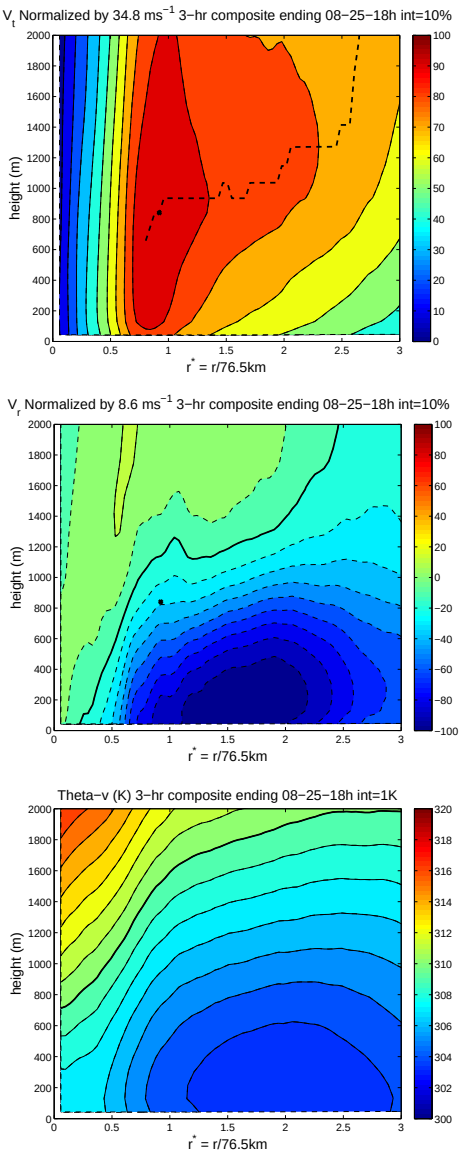

Fig. 8: Azimuthal-mean, time-composited boundary layer structure for the three-hour period ending 18Z August 25, for V_t (top), V_r (middle), and θ_v (bottom). Plots are radially re-scaled by the RMW at z = 2 km. V_t and V_r are normalized by their peak values. The black curves show the height of maximum V_t, height of 10% radial inflow, and 310K, respectively. The small black "x" shows the location of maximum V_t.

lower intensity of the storm or the increased surface friction over nearby land. Interestingly, the location of maximum V_t (small black "x" on the figures) occurs at a slightly greater value of normalized radial inflow, which is more consistent with observations than NRH1.

7. EYEWALL CONVECTION

As in N13, we also present contoured frequency by altitude diagrams (CFADs) for vertical velocity (W), simulated reflectivity (dBZ), and vorticity (ζ) in and near the eyewall of NRH2 around the time of peak intensity. Specifically, distributions of each variable are computed from data points from the period 1800Z Aug 25 to 0000Z Aug 26 in an outward-sloping annulus centered inside the RMW at z = 2 km, which at this time is near r = 60 km. At z = 2 km the annulus ranges from r = 45 to 65 km, and slopes outward above this altitude with a 2:1 ratio (and inward below). Data points with dBZ < 0 are not included in the distributions. As discussed in N13, this configuration is an attempt to allow the best possible comparison with the model data and the CFADs accumulated from observations as presented in Rogers et al. (2012).

Results are shown in Fig. 9 and should be compared to the results for NRH1 and Rogers et al. which are both shown in Fig. 18 of N13. Not surprisingly, the CFADs are quite similar to those shown in N13, but there are a few noteworthy differences. First, the dBZ CFAD for NRH2 is a bit more similar to the observed CFAD, with the axis of peak frequency in dBZ not bending back to lower values at high altitudes as much as for NRH1. The W CFAD has a narrower distribution at low altitudes, perhaps consistent with the lower intensity of the storm, but it has a wider distribution at high altitudes, with considerably more frequent occurrences of W greater than 10 ms^{-1}. These differences in W at higher altitudes may be due to the effect of wind shear concentrating convection in the downshear-left quadrant of the eyewall (Corbosiero and Molinari 2002), the proximity to land proving a source of boundary layer air with somewhat higher CAPE, or some combination of both; further study would be needed to verify these ideas.

8. SUMMARY AND AVAILABLE DATA

Following the work of N13, a second hurricane nature run (HNR2) has been generated using a very similar regional modeling framework. In contrast to HNR1, the tropical cyclone develops and intensifies during significant land interactions, makes landfall on the west coast of Florida, and continues over the southeastern United States. An evaluation of the storm evolution and structure

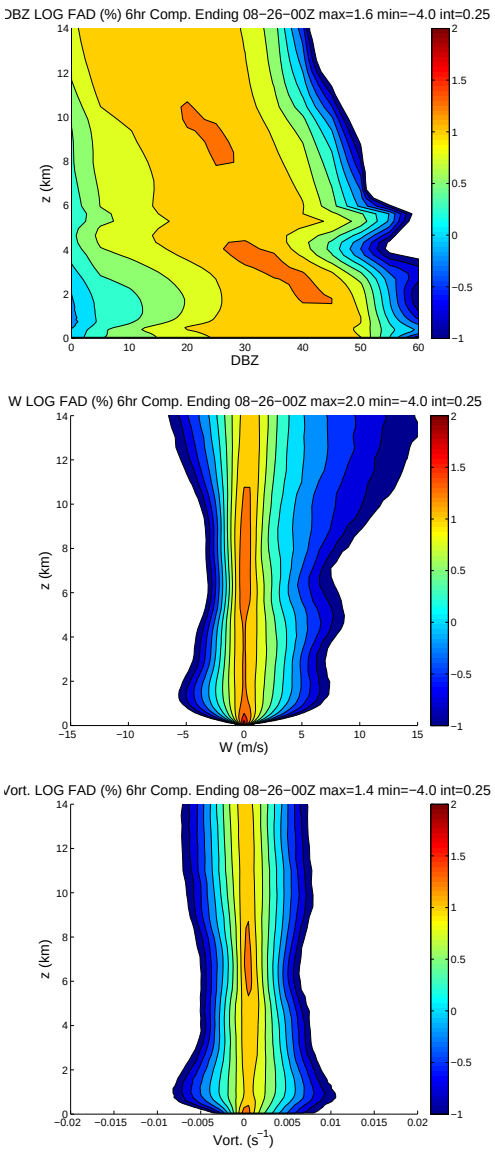

Fig. 9: Contoured frequency by altitude diagrams (CFADs) for simulated reflectivity (top), vertical velocity (middle), an vertical vorticity (bottom) in and inside the eyewall of NRH2 for the 6 hour period ending 00Z August 26. Note that the base-10 logarithm of frequency is actually shown, ranging from -1 (0.1%) to 2 (100%).

confirms that the simulated cyclone has many similarities to composite analyses from real hurricanes and therefore should be useful for generating synthetic observations for OSSEs, and many other research purposes.

All two-dimensional and three-dimensional fields, including all physics tendencies, were saved every 30 min from the 9km and 3km grids, and every 5 min from the 1 km grid, for the entire 8 day simulation. In addition, during the period 12Z August 25 to 12Z August 26, many surface fields of interest (wind speed, surface stress, precipitation rate, etc.) were saved every 10 seconds. All of this data has been archived and is freely available to be used for any purpose.

Acknowledgements:

The authors would like to thank Lisa Bucci for her assistance with processing global data from the Joint OSSE Nature Run. D. Nolan was supported by the NOAA Office of Weather and Air Quality (OWAQ) through its funding of the OSSE testbed at AOML and the NOAA Unmanned Aerial Systems (UAS) Program. C. Mattocks was supported in part by NSF grant AGS-1132646 and by the University of Miami.

References:

Atkinson, G. D., and C. R. Holliday, 1977: Tropical cyclone minimum sea level pressure/maximum sustained wind relationship for the western North Pacific. *Mon. Wea. Rev.*, **105,** 421–427.

Atlas, R., 1997: Atmospheric observations and experiments to assess their usefulness in data assimilation. *J. Meteorol. Soc. Japan*, **75**, 111-130.

Bao, J.-W., S. G. Gopalakrishnan, S. A. Michelson, F. D. Marks, M. T. Montgomery, 2012: Impact of physics representations in the HWRFX on simulated hurricane structure and pressure–wind relationships. *Mon. Wea. Rev.*, **140**, 3278–3299.

Chen, F., and J. Dudhia, 2001: Coupling and advanced land surface-hydrology model with the Penn State-NCAR MM5 modeling system. Part I: Model implementation and sensitivity. *Mon. Wea. Rev.*, **129**, 569-585.

Corbosiero, K. L., and J. Molinari, 2002: The effects of vertical wind shear on the distribution of convection in tropical cyclones. *Mon. Wea. Rev.*, **8**, 2110-2123.

Dvorak, V. F., 1984: Tropical cyclone intensity analysis using satellite data. NOAA Tech. Rep. NESDIS 11, 45 pp.

Kepert, J. D., and D. S. Nolan, 2014: Reply. *J. Atmos. Sci.*, in press.

Knaff, J. A., R. M. Zehr, 2007: Reexamination of tropical cyclone wind–pressure relationships. *Wea. Forecasting*, **22**, 71–88.

Landsea, C. W., and J. L. Franklin, 2013: Atlantic

hurricane database uncertainty and presentation of a new database format. *Mon. Wea. Rev.*, **141**, 3576-3592.

Masutani, M., and Coauthors, 2009: International collaborative joint OSSEs - toward reliable and timely assessment of future observing systems. Preprints, *Anthony J. Hollingworth Symposium*, Phoenix, AZ, Amer. Meteorol. Soc.

Moon, I.-J., I. Ginis, T. Hara, B. Thomas, 2007: A physics-based parameterization of air–sea momentum flux at high wind speeds and its impact on hurricane intensity predictions. *Mon. Wea. Rev.*, **135**, 2869–2878.

Nolan, D. S., R. Atlas, K. T. Bhatia, and L. R. Bucci, 2013: Development and validation of a hurricane nature run using the Joint OSSE Nature Run and the WRF model. *J. Adv. Model. Earth Syst*., **5**, 1-24.

Nolan, D. S., J. A. Zhang, and E. W. Uhlhorn, 2014: On the limits of estimating the maximum wind speeds in hurricanes. *Mon. Wea. Rev.*, in press.

Pollard, R. T., P. B. Rhines,, and R. O. R. Y. Thompson, 1973: The deepening of the wind-mixed layer. *Geophys. Fluid Dyn*., **3**, 381-404.

Rogers, R., S. Lorsolo, P. Reasor, J. Gamache, and F. Marks, 2012: Multiscale analysis of tropical cyclone kinematic structure from airborne Doppler radar composites. *Mon. Wea. Rev*., **140**, 77-99.

Reale, O., J. Terry, M. Masutani, E. Andersson, L. P. Riishojgaard, and J. C. Jusem, 2007: Preliminary evaluation of the European Centre for Medium-Range Weather Forecasts' (ECMWF) Nature Run over the Tropical Atlantic and African Monsoon Region. Geophys. Res. Lett., **34**, L22810, doi:10.1029/2007GL031640.

Tallapragada, V., C. Kieuh, Y. Kwon, S. Trahan, Q. Liu, Z. Zhang, and I.-H. Kwon, 2014: Evaluation of storm structure from the operational HWRF model during 2012 implementation. *Mon. Wea. Rev.*, in press.

Zhang, J. A., R. F. Rogers, D. S. Nolan, and F. D. Marks, Jr., 2011: On the characteristic height scales of the hurricane boundary layer. *Mon. Wea. Rev.*, **139**, 2523-2535.